Liquid-vapor interface, cavitation, and the phase diagram of water

Frédéric Caupin
Laboratoire de Physique Statistique de l'Ecole Normale Supérieure, associé aux Universités Paris 6 et Paris 7 et au CNRS, 24 rue Lhomond 75231 Paris Cedex 05, France

(Received 20 October 2004; revised manuscript received 21 January 2005; published 17 May 2005)

The study of the liquid-vapor interface and of the cavitation phenomenon in water can give deeper insight in its metastable phase diagram. We show how two different equations of state proposed for water, combined with the van der Waals–Cahn-Hilliard theory of a nonuniform system, lead to qualitatively different predictions. In particular, the thickness of the liquid-vapor interface is found either to increase with temperature or to exhibit a minimum. Comparison with available data favors the monotonic behavior and suggests directions for future measurements.

DOI: 10.1103/PhysRevE.71.051605 PACS number(s): 68.03.−g, 64.30.+t, 64.60.Qb

The phase diagram of water is still a matter of debate. The measurements of several thermodynamic anomalies in supercooled water during the 1970s have triggered theoretical attempts to give a unified picture of water in its stable and metastable regions. Speedy [1] proposed that the supercooled region (metastable with respect to the solid formation) and the region where the liquid is stretched (metastable with respect to vapor formation) were bounded by a continuous line of instability. The existence of a line of instability is common to all liquids under tension, and is known as a spinodal line (SL); its generic behavior is that its pressure $P_s(T)$ increases with temperature. In water, $P_s(T)$ could be nonmonotonic; this peculiarity is made possible by the existence of a line of density maxima (LDM). Speedy [1] showed that if the metastable part of the LDM intersects $P_s(T)$, the latter changes slope; $P_s(T)$, negative at room temperature, could then retrace to positive pressure in the supercooled region. This idea is attractive to explain water anomalies, because many properties are singular near a SL. It was later understood [2] that a liquid-gas SL was unlikely to exist at positive pressure in the supercooled region, because it would imply the existence of a second (low temperature) liquid-vapor critical point. The SL can, however, end at negative pressure by meeting a liquid-solid spinodal (see Ref. [2], and references therein) or a glass transition line (see Ref. [3], and references therein).

An alternative interpretation of the anomalies of supercooled water does not involve the SL, but rather postulates the existence of a metastable first-order transition line between a low density and a high density liquid at temperatures below freezing [4]. The critical point terminating this line can also explain the observed anomalies. For a thorough and up-to-date review of supercooled and glassy water, describing these two interpretations and others, we refer the reader to Ref. [2].

The first scenario, with a minimum in $P_s(T)$, is supported by extrapolations at negative pressures of the equation of state (EOS) of water at positive pressure [1]. A careful cavitation experiment [5] using isochoric cooling of water inclusions in quartz was interpreted as an evidence for this behavior. On the other hand, the second scenario, with a second (liquid-liquid) critical point, has been found in all molecular dynamics simulations (MDS) to date (see Ref. [2], and references therein). They predict retracing of the LDM at negative pressure: the LDM thus avoids the SL, and $P_s(T)$ keeps a positive slope. Other experiments, on decompression induced melting in metastable ices, and demonstrating polyamorphism in water (cited in Ref. [2]) were interpreted as supporting the second critical point scenario. Direct experiments on deeply supercooled water would be decisive, but they are precluded by homogeneous crystallization.

In this paper, we concentrate on the temperature variation of $P_s(T)$. A clear understanding of this issue would put more stringent constraints on the models proposed for water. We choose two EOSs with qualitatively different $P_s(T)$. Our aim is to distinguish between them by comparing their predictions for measurable quantities. Experiments are of course difficult to perform close to the limit of stability of the liquid. However, densities out of the stability region are reached in the inhomogeneous situation of liquid-vapor equilibrium. We first derive the predictions of each EOS for the profile of the liquid-vapor interface, and show how experiments favor a monotonic $P_s(T)$. Then, we turn back to the uniform metastable liquid and study the cavitation phenomenon, which is a more direct probe of the spinodal location. We show it is necessary to go beyond the standard theory of nucleation, and we discuss the predictions of each EOS.

Let us first describe the EOSs we use; they were chosen as representative of each scenario mentioned above to explain the anomalies of water. The corresponding SLs are shown in Fig. 1. (i) The Speedy EOS. Speedy [1] has shown that experimental isotherms [6] were accurately represented by the three-parameters formula

$$1-\frac{P}{P_s(T)}=B(T)\left(\frac{\rho}{\rho_s(T)}-1\right)^2. \tag{1}$$

The corresponding $P_s(T)$ exhibits a minimum. (ii) The five-site transferable interaction potential (TIP5P) EOS. We used Eq. (1) to extrapolate the data from Yamada *et al.* [7]. They performed MDS using the TIP5P potential, which is an improvement over the previous ones, as it reproduces a number of features of the phase diagram of water at $P>0$, including the location of the LDM at 1 bar. It also predicts a metastable liquid-liquid critical point. At negative pressures not accessible to experiments, these MDS data lie away from Speedy's extrapolation, and lead to a monotonic $P_s(T)$.

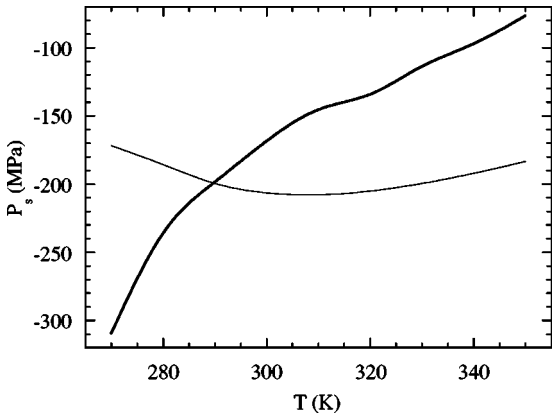

FIG. 1. Spinodal pressure vs temperature. The thin (resp. thick) line is deduced from Speedy (resp. TIP5P) EOS.

Tables I and II of the Appendix give the parameters of Eq. (1).

To describe an inhomogeneous density distribution $\rho(\mathbf{r})$, we use the well-known van der Waals–Cahn-Hilliard (VdW) theory [8]. Given a reference homogeneous liquid at density ρ_l, the excess grand potential of the distribution $\rho(\mathbf{r})$ writes

$$\Delta\Omega = \int_{\mathbb{R}^3} d\mathbf{r}\{\phi(\rho(\mathbf{r}),\rho_l) + \lambda[\nabla\rho(\mathbf{r})]^2\}, \tag{2}$$

where $\phi(\rho,\rho_l)=f(\rho)-f(\rho_l)-f'(\rho_l)(\rho-\rho_l)$ is the excess grand potential density (f is the Helmholtz free energy density) and λ is an influence parameter, accounting for the energy cost associated with inhomogeneous configurations. For a flat interface at equilibrium, $\rho(\mathbf{r})$ varies only along the direction perpendicular to the interface, and connects the equilibrium vapor and liquid densities ρ_v and ρ_l. The grand-potential per unit area reduces to a one dimensional integral. Minimizing $\Delta\Omega$ leads to the equilibrium interface profile and to the surface tension [8]

$$\sigma = 2\int_{\rho_v}^{\rho_l} d\rho\sqrt{\lambda\phi(\rho,\rho_l)}. \tag{3}$$

The profile can be characterized by its 10–90 % thickness

$$l_{10-90} = \int_{0.9\rho_v+0.1\rho_l}^{0.1\rho_v+0.9\rho_l} d\rho\sqrt{\frac{\lambda}{\phi(\rho,\rho_l)}}. \tag{4}$$

The delicate step is the choice of a sound Helmoltz free energy density f for *all* densities. Eq. (1) can be integrated to find f for $\rho\geqslant\rho_s$:

$$f(\rho) = \frac{\rho}{\rho_0}f(\rho_0) + \rho\int_{\rho_0}^{\rho}\frac{P(\rho')}{\rho'^2}d\rho', \tag{5}$$

where $\rho_0\geqslant\rho_s$ is a reference density (e.g., $\rho_0=\rho_l$); the constant $f(\rho_0)$ can be chosen arbitrarily and cancels out in the results. However, for $\rho<\rho_s$, we have to rely on an extrapolation of f. Our first attempt was inspired by a procedure used in the case of liquid helium [9]. First, we set the equilibrium pressure P_{sat} and the vapor density ρ_v to their experimental values [10], and deduce ρ_l from Eq. (1) by solving $P(\rho_l)=P_{sat}$; this value of ρ_l is close to the experimental one (see Table III). Then, we use a fourth order polynomial extrapolation of f. The five coefficients are chosen so that the chemical potential and pressure are equal for ρ_v and ρ_l (phase equilibrium), and that f and its first two derivatives are continuous at ρ_s. Finally, we adjust λ to reproduce the experimental surface tension [10] with Eq. (3). The theory has now no free parameter left, and can be used to predict the liquid-vapor interfacial profile. It is close to an hyperbolic tangent function, as would be the case for a mean field critical limit [8], because the grand potential density $\phi(\rho,\rho_l)$ we obtain is nearly symmetric around $(\rho_v+\rho_l)/2$.

The results for the 10–90 % thickness are shown in Fig. 2. The two EOSs predict qualitatively different behaviors: $l_{10-90}(T)$ obtained with the TIP5P EOS is monotonic, whereas the one obtained with Speedy EOS exhibits a shallow minimum around 320 K. These predictions are compared with experiments: the ellipsometry data from Kinosita *et al.* [11], support the former. The ellipticity measurements were converted into l_{10-90} using Drude theory [12], assuming a hyperbolic tangent function for the density profile. Also shown are the x-ray scattering values [13]; the effective thickness measured by x rays has been converted into total l_{10-90} with the capillary wave theory used by the different authors to analyze their x-ray data. Because of the better accuracy of x rays compared to ellipsometry, it would be interesting to extend x-ray measurements to a wider temperature range. We should also mention that other ellipsometry measurements exist [14], but they are available only at room temperature and were ignored in the comparison. However, as they all give values of l_{10-90} around 0.4 nm, it would be worth repeating a temperature study to confirm the measurements by Kinosita *et al.*

Our first guess for the extrapolation of $f(\rho)$ has an obvious limitation: it does not tend to the ideal gas limit at low density. Therefore we designed a new extrapolation, built to connect the known regions $0\leqslant\rho\leqslant\rho_v$ and $\rho\geqslant\rho_s$. We proceed as follows. We set P_{sat} to its experimental value, and deduce ρ_l from Eq. (1) by solving $P(\rho_l)=P_{sat}$. At low density, we write the pressure as

$$P(\rho) = \frac{RT}{M}\rho\left(1-\frac{\rho}{2\rho_s'}\right), \tag{6}$$

where R is the ideal gas constant, M is the molar mass of water, and ρ_s' is a free parameter. Another spinodal (for the transition from the gas to the liquid) arises, at a density ρ_s' and a pressure $P_s'=RT\rho_s'/(2M)$. For densities between ρ_s' and ρ_s, we take a third order polynomial for $P(\rho)$. In each of the three regions $\rho\leqslant\rho_s'$, $\rho_s'\leqslant\rho\leqslant\rho_s$, and $\rho\geqslant\rho_s$, an expression for $f(\rho)$ is obtained using Eq. (5). This gives three constants of integration, one of which can be given an arbitrary value. Along with ρ_v, ρ_s', and the coefficients of the polynomial for $P(\rho)$, eight independent parameters remain. They are fully determined by the following eight conditions: the chemical potential and pressure are equal for ρ_v and ρ_l (phase equilibrium), and f and its first two derivatives are continuous at ρ_s' and ρ_s. We note that the result obtained for ρ_v is in good agreement with the experimental value [10] (see Table III).

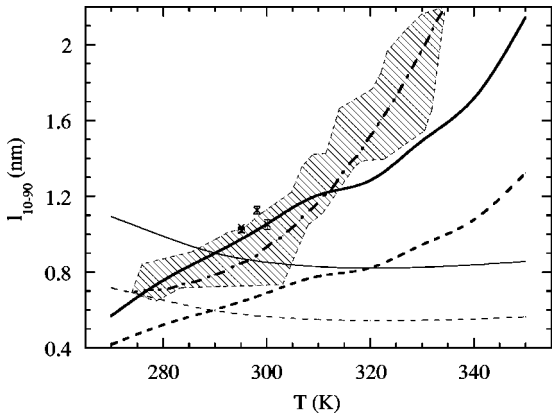

FIG. 2. 10%–90% thickness of the liquid-vapor interface of water vs temperature. The thin solid (resp. dashed) line was calculated using Speedy EOS, and the thick solid (resp. dashed) line using TIP5P EOS with our first (resp. second) extrapolation for $f(\rho)$ (see Table IV). The thick dash-dotted line represents the ellipsometry measurements from Kinosita *et al.* (see Ref. [11]), and the hatched area indicates the scatter of the data. The crosses (with error bars) show the values derived from several x-ray scattering experiments (see Ref. [13]).

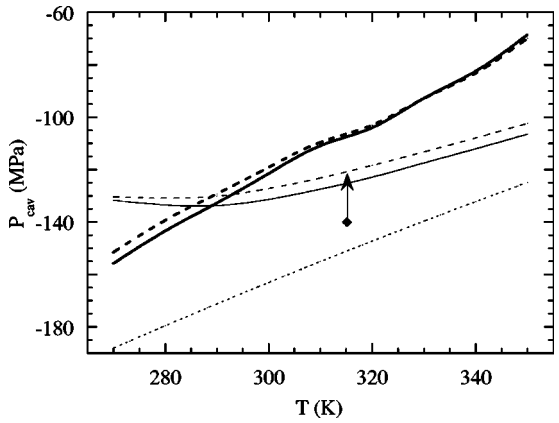

FIG. 3. Cavitation pressure vs temperature. The dotted line shows the prediction of the TWA. The thin solid (resp. dashed) line was calculated using Speedy EOS, and the thick solid (resp. dashed) line using TIP5P EOS with our first (resp. second) extrapolation for $f(\rho)$ (see Table IV). The filled diamond is the largest tension at which cavitation was observed in a quartz inclusion (see Ref. [5]); P_{cav} is calculated assuming that the volume of the inclusion remains constant; the arrow indicates the correction due to the matrix compliance effect.

Predictions for l_{10-90} from our two extrapolations of $f(\rho)$ can be compared to check the sensitivity of our results to the model. As shown in Fig. 2, for both EOSs, the second extrapolation gives results systematically lower than the first one. However, the qualitative temperature dependence of l_{10-90} appears to be a robust feature of our model. Therefore, our conclusion that the monotonic behavior of the available experimental measurements favor the TIP5P EOS is unaffected.

Another, more direct, way to approach the SL and to distinguish between the two EOSs proposed, is to study cavitation in the stretched liquid. Because the liquid-gas transition is first order, any liquid can be brought to negative pressures, into a metastable state separated from the stable gas phase by an energy barrier E_{b}. This barrier vanishes on the SL, where the liquid state becomes unstable. Yet the spinodal pressure cannot be reached because thermal fluctuations will allow a gas bubble to nucleate before, overcoming a finite E_{b} at the cavitation pressure P_{cav}. For a liquid free of impurities, cavitation is called homogeneous, and the corresponding E_{b} can be estimated as $k_{\mathrm{B}}T\ln(\Gamma_0 V\tau/\ln 2)$, where V and τ are the characteristic volume and time of the experiment. Γ_0 is evaluated as the product of the number density of independent nucleation sites, $1/(4\pi R_{\mathrm{c}}^3/3)$ (R_{c} is the radius of the critical nucleus for nucleation, for which E_{b} is reached, typically 1 nm in our calculations) by a thermal attempt frequency $k_{\mathrm{B}}T/h$. Note that E_{b} depends only weakly on the choice of $\Gamma_0 V\tau$. The pressure dependence of E_{b} may be found using the so called thin wall approximation (TWA) [15], which consists in treating the growing nucleus as a spherical bubble of radius R, filled with vapor at the saturated vapor pressure P_{sat}, and separated from the liquid by abrupt walls. Its energy is thus divided into a volume and a surface term

$$E(P) = 4\pi R^2\sigma + \tfrac{4}{3}\pi R^3(P - P_{\mathrm{sat}}) \tag{7}$$

and results in a barrier $E_{\mathrm{b}} = 16\pi\sigma^3/[3(P-P_{\mathrm{sat}})^2]$ at $R_{\mathrm{c}} = 2\sigma/(P_{\mathrm{sat}}-P)$. This simple theory does not predict a vanishing barrier at a finite negative pressure, although this must occur on the SL. The reason is that the assumption of a sharp wall fails when R_{c} becomes of the order of l_{10-90}. To solve this problem, we resort to VdW theory of nucleation [16]. Let us consider a given negative pressure, corresponding to a metastable homogeneous liquid at density ρ_{l}. The excess grand potential $\Delta\Omega$ of an inhomogeneous density distribution $\rho(\mathbf{r})$ is written with Eq. (2). Among the profiles connecting asymptotically to ρ_{l}, one makes $\Delta\Omega$ stationary: this value of $\Delta\Omega$ defines E_{b}. The corresponding critical profile is found by solving the associated Euler-Lagrange equation

$$2\lambda\Delta\rho = \frac{\partial\phi}{\partial\rho}. \tag{8}$$

This was done using both EOSs, to find $P_{\mathrm{cav}}(T)$; we used typical experimental parameters: $V=(10\ \mu\mathrm{m})^3$ and $\tau=1$ s [5]. The results are shown in Fig. 3. Again, the two EOSs predict qualitatively different behaviors: when Speedy EOS is used, $P_{\mathrm{cav}}(T)$ exhibits a shallow minimum around 285 K, whereas $P_{\mathrm{cav}}(T)$ deduced from TIP5P is monotonic. These features hold for both extrapolations mentioned above: P_{cav} is less negative when the second extrapolation is used, but the difference is smaller than for l_{10-90}. The discrepancy between TWA and VdW theory appears also clearly: the TWA always overestimates the cavitation pressure.

We have included in Fig. 3 one data point from Zheng *et al.* [5]. They used a Berthelot tube technique. Quartz inclusions were filled with liquid water through cracks in the quartz crystal; these cracks were then healed at high temperature; during cooling, the low-density water sample fol-

TABLE I. Parameters of Eq. (1) for Speedy EOS.

T (K)	$-P_s$ (MPa)	ρ_s (kg m^{-3})	B	RMSD(P) (MPa)
270[a]	171.9	823.13	21.7057	0.044
280	185.7	817.78	20.1659	0.031
290	199.5	812.70	19.0743	0.023
300	206.5	810.23	18.9109	0.019
310	207.9	809.44	19.3667	0.015
320	205.2	809.53	20.2512	0.013
330	199.6	809.84	21.4308	0.011
340	192.1	809.95	22.8113	0.010
350	183.5	809.61	24.3364	0.009

[a]Although this temperature lies slightly out of the range of the data from Ref. [6], we used their EOS which extrapolates smoothly into this region.

TABLE II. Parameters of Eq. (1) for TIP5P EOS.

T (K)	$-P_s$ (MPa)	ρ_s (kg m^{-3})	B	RMSD(P) (MPa)
270	309.4	701.91	5.45980	8.6
280	236.1	769.46	10.8780	6.8
290	198.4	803.27	16.4810	5.4
300	168.5	822.70	22.5113	4.9
310	145.4	834.39	28.8860	4.9
320	134.2	835.43	32.2850	4.6
330	113.7	840.50	40.2859	5.0
340	97.12	841.42	48.4521	3.4
350	76.50	847.30	65.8575	4.8

lowed a nearly isochoric path, and eventually a bubble nucleated. Zheng *et al.* reported a maximum tension at room temperature, corresponding to the datum in Fig. 3. They were able to cool down further other inclusions, without observing cavitation. They concluded that the isochore was retracing to less negative pressure, and interpreted this as the evidence that the LDM extends down to the SL, which supports Speedy's model.

It is tempting to check this by comparing directly the experimental P_{cav} to our predictions. Unfortunately, the pressure is difficult to calibrate in such experiments: the experimentally measured quantity is the cavitation temperature, and P_{cav} is deduced by the use of yet another EOS and an assumption about the volume of the inclusion. To distinguish between the two predictions, it would be useful to obtain the temperature dependence of P_{cav}. As this seems difficult to do at lower temperature with inclusions, we plan to use an acoustic technique that gave evidence for a minimum in $P_s(T)$ in liquid helium 3, which also exhibits a LDM [17].

We should mention that a third interpretation for water anomalies exists: the singularity free scenario [2]. It explains the increases of response functions upon supercooling as thermodynamical consequences of the existence of density anomalies. This was illustrated by two theoretical models [18]. We did not consider the corresponding EOSs here, but as they both predict a monotonic $P_s(T)$, we expect calculations of $l_{10-90}(T)$ and $P_{cav}(T)$ to give results qualitatively similar to TIP5P.

Competing pictures exist for the phase diagram of water. They differ in several ways, one of which is the shape of the liquid-gas SL. We have shown that this issue could be checked experimentally. The measured temperature dependence of the thickness of the free surface of water seems to support a monotonic $P_s(T)$. More x rays and ellipsometry measurements as a function of temperature are needed to confirm this finding. However, the interfacial profile spans all densities between the stable liquid and gas phases; a more direct test of the spinodal shape could be obtained by measuring the temperature dependence of homogeneous cavitation at low temperature, when metastable liquid densities close to the spinodal are reached.

TABLE III. Density functional parameters.

T (K)		270[a]	280	290	300	310	320	330	340	350
P_{sat} (Pa)	Exp.	484.7	991.8	1919.9	3537	6231.2	10546	17214	27190	41680
ρ_v (kg m^{-3})	Exp.	0.003892	0.0768	0.01436	0.02559	0.04366	0.0717	0.1136	0.1744	0.2603
	S2	0.003911	0.00771	0.01440	0.02565	0.04377	0.0719	0.1139	0.1750	0.2615
	T2	0.003891	0.00768	0.01440	0.02577	0.04423	0.0729	0.1168	0.1815	0.2770
ρ_1 (kg m^{-3})	Exp.	999.48	999.86	998.75	996.51	993.34	989.38	984.74	979.50	973.70
	S1-S2	999.81	999.89	998.79	996.54	993.37	989.42	984.79	979.55	973.75
	T1-T2	1002.31	1002.76	1001.14	996.10	989.64	982.47	972.93	962.32	951.74
ρ_s' (kg m^{-1})	S2	0.3593	0.8256	1.738	2.9664	4.355	5.783	7.201	8.608	10.02
	T2	10.86	2.871	1.423	1.8618	1.435	1.763	1.817	1.999	2.026
σ (mN m^{-1})	Exp.	76.1	74.7	73.2	71.7	70.1	68.5	66.8	65.0	63.2
λ (10^{-17} m^7 kg^{-1} s^{-2})	S1	5.69	5.05	4.51	4.20	4.02	3.93	3.89	3.89	3.91
	S2	3.63	3.23	2.90	2.70	2.59	2.53	2.50	2.50	2.51
	T1	2.88	3.81	4.48	5.20	5.91	6.23	7.21	8.25	10.2
	T2	2.00	2.52	2.90	3.31	3.73	3.91	4.49	5.10	6.27

[a]Although this temperature lies slightly out of the range of experimental data, we used the formulas of Ref. [10] which extrapolate smoothly into this region.

TABLE IV. Calculated interfacial thicknesses and cavitation pressures.

T (K)		270	280	290	300	310	320	330	340	350
l_{10-90} (nm)	S1	1.093	0.989	0.900	0.851	0.828	0.821	0.825	0.838	0.856
	S2	0.716	0.651	0.596	0.564	0.549	0.544	0.545	0.552	0.563
	T1	0.568	0.755	0.899	1.052	1.206	1.283	1.492	1.715	2.144
	T2	0.416	0.521	0.601	0.689	0.777	0.821	0.943	1.074	1.323
$-P_{cav}$ (MPa)	TWA	188.1	179.6	171.2	163.1	155.1	147.3	139.7	132.2	124.9
	S1	131.7	133.5	133.7	131.4	127.5	122.9	117.5	112.1	106.5
	S2	130.3	130.8	130.1	127.2	123.2	118.4	113.3	107.9	102.4
	T1	155.8	143.5	132.7	121.5	110.9	104.0	92.8	82.5	68.6
	T2	151.6	139.4	129.3	119.1	109.6	103.0	92.9	83.2	69.9

I wish to thank P. Kumar, H. E. Stanley, and M. Yamada for providing me with the TIP5P data, and M. Barranco, D. Bonn, A. Boudaoud, J. Meunier, S. Rafai, E. Rolley, and H. E. Stanley for helpful discussions.

APPENDIX: TABLES OF PARAMETERS

We list here the values of all parameters used in our calculations. Let us first give the parameters appearing in Eq. (1) for the two EOSs considered. (i) The Speedy EOS (Table I): following Speedy [1], we have fitted at each temperature 11 experimental values of $P(\rho)$ [6] at 10 MPa intervals in the range 0–100 MPa; the root mean square deviation in the pressure [RMSD(P)] is comparable to the experimental uncertainty. (ii) The TIP5P EOS (Table II): we used at each temperature seven densities equally spaced between 900 and 1200 kg m^{-3} (the corresponding pressure ranges vary from −180–550 MPa at 270 K to −60–800 MPa at 350 K); RMSD(P) is larger than for Speedy EOS, but still smaller than the numerical uncertainty in the TIP5P calculation (see the inset in Fig. 1 of Ref. [7]).

Table III lists other parameters that appear in the functional (P_{sat}, ρ_v, ρ_s, ρ_s', σ, and λ). In the labels, the letter S (respectively, T) stands for Speedy (respectively, TIP5P) EOS, the number 1 (respectively, 2) for the first (respectively, second) kind of extrapolation of the Helmoltz free energy in the unstable region. As the functional parameters are chosen to reproduce P_{sat} and σ (and also ρ_v for the first kind of extrapolation), we give only the experimental values of these quantities; for the others, we compare the experimental values to the functional parameters.

Finally, we give in Table IV the results obtained with the different EOSs and extrapolations for the interfacial thickness l_{10-90} and for the cavitation pressure P_{cav}, as plotted in Figs. 2 and 3.

[1] R. J. Speedy, J. Phys. Chem. **86**, 3002 (1982).
[2] P. G. Debenedetti, J. Phys.: Condens. Matter **15**, R1669 (2003).
[3] R. J. Speedy, J. Chem. Phys. **120**, 10182 (2004).
[4] P. H. Poole, F. Sciortino, U. Essmann, and H. E. Stanley, Nature (London) **360**, 324 (1992).
[5] Q. Zheng, D. J. Durben, G. H. Wolf, and C. A. Angell, Science **254**, 829 (1991).
[6] C.-T. Chen, R. A. Fine, and F. J. Millero, J. Chem. Phys. **66**, 2142 (1977).
[7] M. Yamada, S. Mossa, H. E. Stanley, and F. Sciortino, Phys. Rev. Lett. **88**, 195701 (2002).
[8] J. W. Cahn and J. E. Hilliard, J. Chem. Phys. **28**, 258 (1958).
[9] Q. Xiong and H. J. Maris, J. Low Temp. Phys. **77**, 347 (1989).
[10] The International Association for the Properties of Water and Steam, Supplementary release: saturation properties of ordinary water substance, September 1992. URL: http://www.iapws.org/relguide/supsat.pdf. Release on the surface tension of ordinary water substance, September 1994. URL: http://www.iapws.org/relguide/surf.pdf
[11] K. Kinosita and H. Yokota, J. Phys. Soc. Jpn. **20**, 1086 (1965); K. Kinosita and S. Kawabata, Opt. Acta **26**, 931 (1979).
[12] P. W. Drude, *Theory of Optics* (Longmans Green, New York, 1902), p. 292.
[13] A. Braslau, P. S. Pershan, G. Swislow, B. M. Ocko, and J. Als-Nielsen, Phys. Rev. A **38**, 2457 (1988); J. Daillant, L. Bosio, J. J. Benattar, and J. Meunier, Europhys. Lett. **8**, 453 (1989); D. K. Schwartz *et al.*, Phys. Rev. A **41**, 5687 (1990); Y. F. Yano and T. Iijima, J. Chem. Phys. **112**, 9607 (2000).
[14] Lord Rayleigh, Philos. Mag. **33**, 1 (1892); C. V. Raman, and L. A. Ramdas, *ibid.* **3**, 220 (1927); C. Bouhet, Ann. Phys. (Paris) **15**, 5 (1931); J. M. Bain, R. C. Bacon and H. D. Bruce, J. Chem. Phys. **7**, 818 (1939); D. Beaglehole, J. Phys. Chem. **91**, 5091 (1987).
[15] J. C. Fisher, J. Appl. Phys. **19**, 1062 (1948).
[16] J. W. Cahn and J. E. Hilliard, J. Chem. Phys. **31**, 688 (1959).
[17] F. Caupin, S. Balibar, and H. J. Maris, Phys. Rev. Lett. **87**, 145302 (2001).
[18] S. Sastry, P. G. Debenedetti, F. Sciortino, and H. E. Stanley, Phys. Rev. E **53**, 6144 (1996); T. M. Truskett, P. G. Debenedetti, S. Sastry, and S. Torquato, J. Chem. Phys. **111**, 2647 (1999).